Rev Anal Chem 31 (2012): 1–6 © 2012 by Walter de Gruyter • Berlin • Boston. DOI 10.1515/REVAC.2011.122

Phase aspects of (broadband) stimulated Raman scattering

Herman L. Offerhaus*, Erik T. Garbacik, Alexander C.W. van Rhijn, Andrew L. Fussell, and Jennifer L. Herek

Optical Sciences Group, University of Twente, Science and Technology, P.O. Box 217, Enschede 7500 AE, The Netherlands, e-mail: H.L.Offerhaus@utwente.nl

*Corresponding author

Abstract

The phase of the molecular response can be exploited to improve selectivity without sacrificing speed in both narrowband and broadband coherent anti-Stokes Raman scattering (CARS) microscopy, both of which will be considered in this review of the work that was performed in our group.

Keywords: coherent control; microscopy; nonlinear optics.

Introduction

Vibrational microscopy has two goals: speed and selectivity (Zheltikov et al. 2009, Xie et al. 2011). The ideal system would combine both goals, but in general a compromise must be struck. The trade-off presents itself as a balance between spectral information and imaging speed. The spectral information is gathered per pixel and this requires integration time or scanning that limits the overall speed. At the extremes of this balance we find spontaneous Raman imaging in one corner with full spectral information, linear concentration dependence and low speed. The other corner is occupied by narrowband coherent anti-Stokes Raman scattering (CARS) with just one spectral discriminating line, quadratic concentration dependence and a non-resonant background, but with tremendous speed. In between we find a variety of techniques such as spectrally scanning CARS (Ganikhanov et al. 2006, Kano 2010), amplitude shaped stimulated Raman scattering (SRS) (Xie et al. 2011) and different incarnations of broadband CARS (Rinia et al. 2007, Motzkus et al. 2009, Parekh et al. 2010). In the Optical Sciences Group at the University of Twente we have pursued the use of phase to improve selectivity without sacrificing speed in both narrowband and broadband CARS, both of which will be considered in this review. This is not intended to be a broad review of the field just of the work in our group and the framework in which we understand that work.

The molecular response function

The phase response that is probed in SRS can be intuitively understood as the response of the driven harmonic oscillator, where the driving field is given by the difference frequency of the pump and Stokes fields. Strictly speaking, this field at the difference frequency is not present itself, nor does it interact with the usual dipole transition moments. Its effect can only be experienced by something with a nonlinear response and it interacts with Raman active transitions rather than infrared active transitions. However, once these conditions are fulfilled, the response of the system is just like the response of a linear harmonic oscillator to a driving force: there is an amplitude profile with a peak and a phase change over the resonance, all described by a complex Lorentzian profile. The phase in this profile indicates the phase of the polarization with respect to the phase of the driving field. At a frequency below the resonance the polarization follows the driving field closely, at the resonance frequency the polarization lags the driving field by 90° and above the resonance frequency the polarization lags by 180°. In the complex plane, the response function for a single isolated resonance as a function of frequency describes a perfect circle (Lucassen 1992). When multiple resonances are present and partially overlap, a complicated trajectory through the complex plane results, as shown in Figure 1.

This complex response is probed by the probe field and the phase is therefore present in the output field. An interferometric measurement will reveal this phase with respect to the local oscillator. For narrowband CARS measurements, the polarization that is generated is given by:

$$P_{CARS} \propto E_{pump} E^{*}_{Stokes} E_{probe} \chi^{(3)}_{pump\text{-}Stokes}. \quad (1)$$

The light that is emitted due to the induced polarization is 90° out of phase with the induced polarization itself (it is the derivative of the motion that causes emission, not the motion itself) so that the phase of the generated CARS can be expressed as:

$$\varphi_{CARS} = \varphi_{pump} - \varphi_{Stokes} + \varphi_{probe} + \varphi_{\chi^{(3)}_{pump-Stokes}} + \pi \quad (2)$$

as the anti-Stokes wavelength is set apart from the input fields, a local oscillator has to be supplied to reveal the phase (Potma et al. 2006). For SRS, where the output wavelength coincides with the input fields, the interference is directly with the input field. The polarization is given by:

$$P_{SRS}(\omega_{pump}) \propto E_{pump} E^{*}_{Stokes} E_{Stokes} \chi^{(3)}_{Pump\text{-}Stokes} = E_{pump} \left| E_{Stokes} \right|^2 \chi^{(3)}_{Pump\text{-}Stokes}. \quad (3)$$

And the phase is given by:

$$\varphi_{SRS}(\omega_{pump}) = \varphi_{pump} - \varphi_{Stokes} + \varphi_{Stokes} + \varphi_{\chi^{(3)}_{Pump-Stokes}} + \pi = \varphi_{pump} + \varphi_{\chi^{(3)}_{Pump-Stokes}} + \pi \quad (4)$$

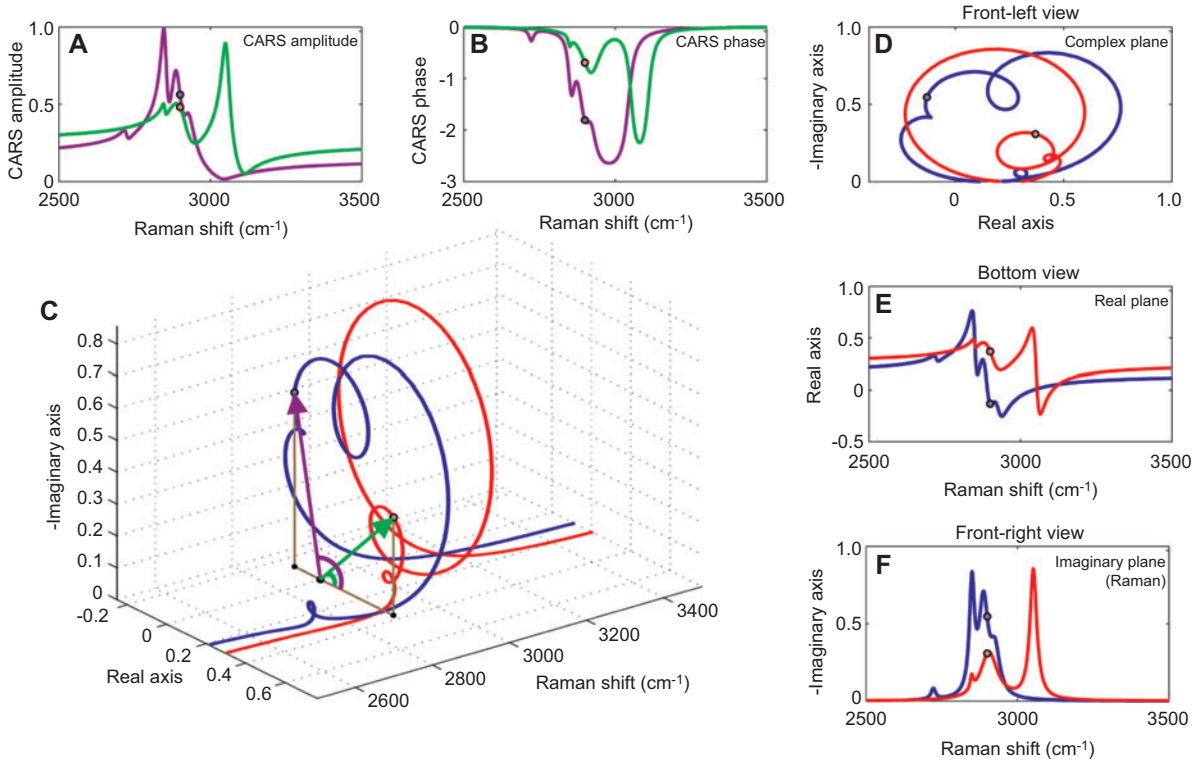

Figure 1 The trajectories of the vibrational responses of polyethylene and polystyrene through complex space near 3000 cm^{-1}. The amplitudes (A) and phases (B) of the CARS responses of these two plastics are shown in violet and green, respectively. When the amplitude and phase are plotted as a function of the driving frequency, the spirals in part (C) are constructed. Projections along each axis of this 3D space are shown on the right side and correspond to the full complex trajectory (D, projection along the frequency axis), the real component of the complex response as a function of frequency (E, projection along the imaginary axis), and the background-free Raman spectrum (F, projection along the real axis). The small circles in each figure correspond to the locations of polyethylene and polystyrene at 2900 cm^{-1}, respectively.

so that the interference of this light with the original incident light is fully destructive at resonance (twice 90°). In other words, the imaginary part of the response destructively interferes with the incoming field so that it is observed as an absorption. The real part of the interference causes a phase shift that can be interpreted as a change in the refractive index. As the absolute phase is generally not accessible (in narrowband experiments), it is impossible to measure this part and thus extract the full phase without additional information or assumptions. In broadband experiments, the phase profile is revealed over a broad frequency range so that the phase at resonance can be compared to the phase around the resonance to establish a "base" value.

Narrowband CARS and SRS

For a measurement at a single frequency, the response of a material is given by some position in the complex plane. It is clear that two-dimensional information about this position, along two axes (real and imaginary), is worth more than information along just one axis. One important advantage is the fact that the non-resonant response must be real and therefore lies along the real axis. When the measured signal is projected along the imaginary axis, the background is rejected and only the resonant information remains.

When a sample contains multiple substances that have overlapping resonances, the amplitudes could be the same, making it difficult to distinguish them, whereas the phases can be somewhat different and allow for their discrimination. By recording the phase different (pure) components can be identified and mixtures can be unraveled (Jurna et al. 2010, Orsel et al. 2010). An example of a combination of pure substances in one sample is shown in Figure 2.

Narrowband SRS (Volkmer et al. 2009, Saar et al. 2010) is often described as "background free" compared to CARS so that the detection of the phase to remove a background would seem superfluous. However, identification of mixtures (or concentrations of reaction products) by measuring only amplitudes is not straightforward when more than two components are present. Detection of the total phase of SRS is complicated by the fact that the local oscillator in SRS is the same beam as the pump (or Stokes) so that the frequency of this beam cannot be shifted independently to create a heterodyne measurement. Our solution to this has been to "move the interference to the vibrational level"; instead of driving the vibration through one pathway, we drive through two competing pathways that have a time-varying phase relation (Jurna

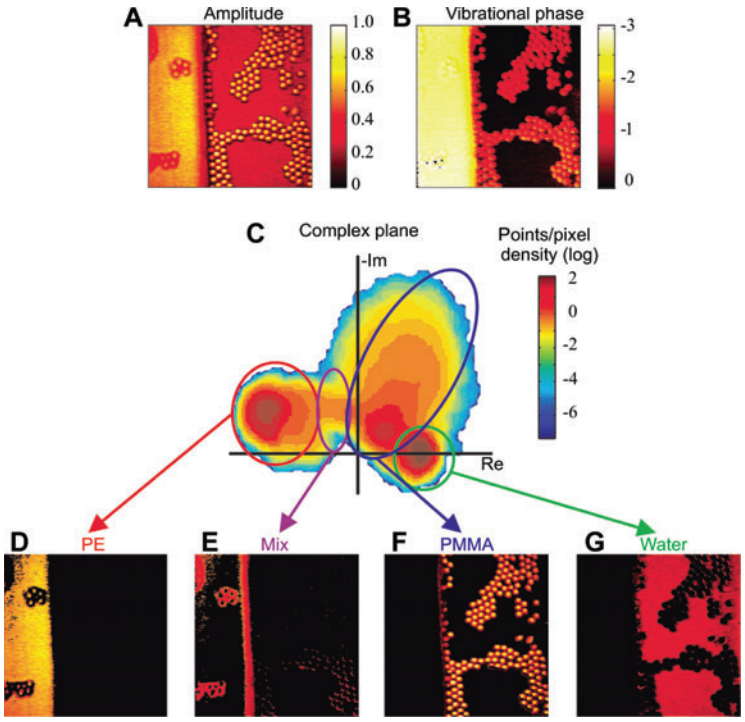

Figure 2 Measurement of the amplitude and phase at each location in a sample allows identification of the individual components. Top: amplitude (A) and vibrational phase (B) of a sample containing a sheet of PE, 4 μm PMMA beads, and water, imaged at 2940 cm^{-1}. Middle: density graph of the projected amplitude and vibrational phase points in the complex plane (C). Bottom: multicomponent analysis, where the different components (D–G) are separated by their location in the complex plane. The "mix" plot shows regions of the image where two or more components are represented in the same focal volume. Each image is 100 μm×100 μm.

et al. 2009) (they β). The molecule thus experiences a modulated total driving field as the two fields rotate in and out of phase. The amplitude modulation of the total driving field is revealed through the amplitude (or intensity) of a co-existing CARS process (see Figure 3, labeled as ω_{as}). This anti-Stokes signal carries the phase of the driving fields before interaction with the molecule. The phase of the response is seen in the interference in the SRS signal which includes the effect of the molecular response on the driving field. An interesting side effect of this approach is that the absence of amplitude modulation of the input beams causes insensitivity to Kerr-lensing or thermal effects that can cause non-resonant artifacts in SRS (Garbacik et al. 2011).

Compared to other CARS approaches and SRS, the method that we have developed for measuring the phase does not reduce the imaging speed. Integration times are on the order of 1 μs/pixel so that full 256×256 images are collected in seconds. We also do not need any additional excitation sources but use the same optical parametric oscillator (OPO). The setup is however more complex. As there is a third wavelength in focus, the requirements on the alignment and the level of chromatic aberrations is more stringent. If background rejection is not an issue, regular CARS is easier. If background rejection is required but the samples are fairly simple, SRS might be an easier alternative. If the samples are complex, a minority component has to be measured and different resonances overlap; our phase approach will allow for a greater selectivity without loss of speed.

Broadband phase shaped CARS and SRS

There are many ways to implement broadband CARS or SRS (Oron et al. 2004, McGrane et al. 2009, Umapathy et al. 2009, Gilch et al. 2010, Day et al. 2011, Lee et al. 2011). Two specific implementations will be discussed here: broadband CARS where the pump and probe are broad but the Stokes is narrow and broadband SRS where the pump is narrow and the Stokes is broad. The reason for these choices is as follows: if both the pump and Stokes are broadband pulses, the shaping on these pulses is mixed (convoluted) in their interaction and the driving field at the difference frequency becomes a very complicated function of the originally imposed shape. If, however, one of these fields is narrow, the shape that is imposed on the broadband pulse is shifted to the frequency difference without significant alteration. This has the significant advantage that the shape that is imposed on the pulse interacts directly with the molecule. In many cases the amplitude and phase of the response function of these molecules is known, so this molecular phase can be addressed (changed, compensated or enhanced) by the imposed shaping. This approach is not unlike the matched filter technology that was originally developed for radar but in this case we match the optical pulse shape to the molecular response (North 1943, Turin 1960).

For the broadband CARS situation the induced polarization cannot be expressed as a multiplication in the frequency domain, as in Eq. (1), but must be expressed as a convolution

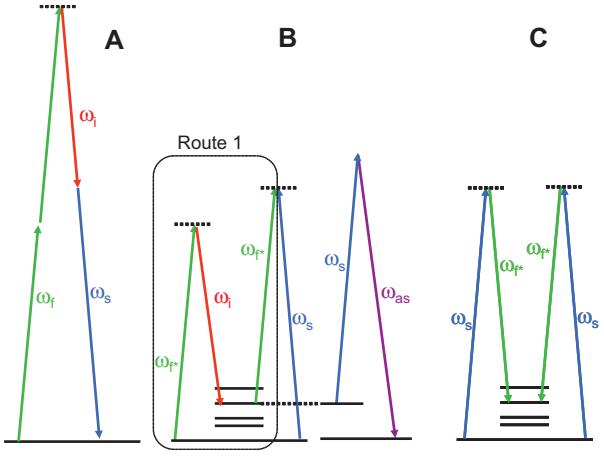

Figure 3 The phase preserving chain for heterodyne detection of CARS and SRS. (A) The SHG and OPO process with the fundamental (ω_f) that generates a second harmonic which in turn creates the signal (ω_s) and idler (ω_t). After the OPO, the fundamental is frequency shifted by 1 MHz by an AOM (ω_{f*}). (B) The fundamental (ω_{f*}) – the Idler (ω_i) coincides with the Signal (ω_s) – the fundamental (ω_{f*}) with a frequency difference of 2 MHz. The amplitude of the resulting driving field is probed by the signal and creates an anti-Stokes (ω_{as}) that can be monitored separately to probe the local driving phase. Route 1 indicates the pathway $[(\omega_{f*}-\omega_i)\chi^{(3)}+\omega_{f*}]$ that creates an interference on the signal. Interference on the idler is created by the CSRS pathway of $-(\omega_s-\omega_{f*})\chi^{(3)}+\omega_{f*}$. Interference on the fundamental (ω_{f*}) is created from two sides. Panel (C) shows the conventional pathway for interference on the signal; however, as there is no amplitude modulation and the frequency (or phase) modulation cancels, no modulation is seen at 2 MHz.

of the driving fields. As we use a narrow Stokes field (narrow with respect to the resolution of the shaping), we can still assume the Stokes to be a δ function in frequency so that the convolution reduces to a frequency shift and the CARS polarization reduces to:

$$P(\omega)\infty E^*_{Stokes}(\omega_{Stokes})\cdot\left[E_{pump}(\omega+\omega_{Stokes})\cdot\chi^{(3)}(\omega)\right]\otimes E_{pump}(\omega). \quad (5)$$

This result could loosely be described by saying that the spectrum of the (shaped) pump field is shifted to the difference frequency where it is multiplied by the molecular response function and subsequently convoluted with the (shaped) pump field so that a field at the (optical) CARS frequencies is generated. Owing to that second convolution, the result is only partly intuitive. However, a few special cases do yield predictable outcomes: if no shape is imprinted, the molecular response function is (more or less) multiplied by a constant (or slowly varying envelope function) so that its phase profile remains unchanged. The subsequent convolution with the (unshaped) pump field will smear out the spectral features of the molecular response over the width of the pump field so that a broad featureless spectrum is produced. If the shape that is imprinted on the pump field is the complex conjugate of the molecular response then the multiplication results in a function with an amplitude profile that resembles the molecular profile and a flat phase, corresponding to a relatively short pulse in time. The subsequent convolution with the (shaped) pump pulse will generate a broad pulse where the parts of the pump spectrum that did not contain a lot of shaping will contribute to a short intense pulse. In other words, to obtain a large overall response it is advantageous to shape the pump with some function that is close to the complex conjugate of the molecular response function.

The precise function required for an optimum response depends on the spectral width of the pump and the balancing of the shaped and unshaped parts. We have used an evolutionary optimization routine to find these optimal phase shapes (van Rhijn et al. 2011, Yang et al. 2011). To avoid ending up with a fully non-resonant optimization we do not use the absolute signal strength as a measure of the fitness. Instead, we use the difference of the signal for the shaped pump and the signal for the pump shaped with the complex conjugate of the shaping function. A purely non-resonant response will yield the same result for both cases so that the fitness goes to zero. One result for an optimal shape is shown in Figure 4.

For broadband SRS (again with just one broadband and one narrowband input), it might seem like the interaction with a broad Stokes or pump would always result in a broad convoluted response, but this is not necessarily true. In the situation depicted in Figure 5, the broadband Stokes excites a wide range of vibrations. This entire spectrum interacts with the Stokes again which indeed induces a polarization over a wide frequency range (the light red area), but to overlap with the narrow pump, and be amplified through interferometric amplification of that pump, the frequencies interacting with the molecular response function are exactly those (indicated in dark red) that also interacted with the pump in the first place to excite the same part of the vibrational spectrum.

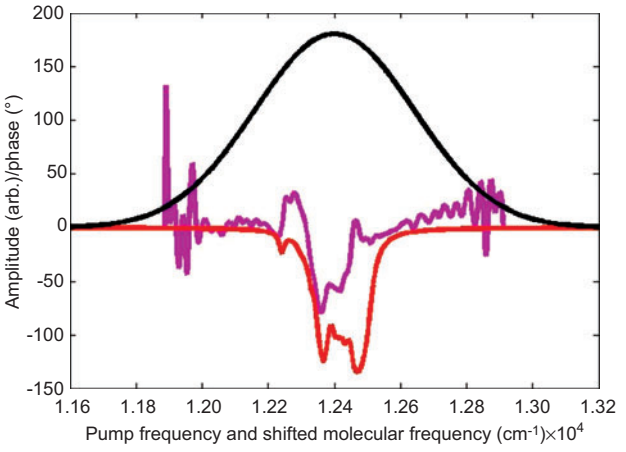

Figure 4 Optimized phase profile (in purple) to extract an optimal signal from a PMMA molecule, given a Gaussian pump profile (black). The phase of the molecular response of PMMA is shown in red. The optimum shaping function follows the molecular features but not completely.

$$P(\omega)\infty\left[E^{*}_{Stokes}(\omega_{Pump}-\omega)\cdot E_{Pump}(\omega_{Pump})\cdot\chi^{(3)}(\omega)\right]\otimes E_{Stokes}(\omega)\Rightarrow$$
$$P(\omega_{Pump})\infty E_{Pump}(\omega_{Pump})\int_{\omega_{Stokes}} E^{*}_{Stokes}(\omega)\cdot\chi^{(3)}(\omega_{Pump}-\omega)\cdot E_{Stokes}(\omega)\,d\omega=$$
$$E_{Pump}(\omega_{Pump})\int_{\omega_{Stokes}}\left|E_{Stokes}(\omega)\right|^{2}\chi^{(3)}(\omega_{Pump}-\omega)\,d\omega \qquad (6)$$

In other words, the light that is seen to interfere with the pump is light that used the same part of the broadband Stokes to both excite and probe a vibration, see Figure 5. The driving field at the difference frequency is given by the interaction of the narrow pump and the broad (shaped) Stokes, and – similar to the shaped CARS case – this amounts to a shift of the Stokes spectrum to the difference frequency. At the difference frequency it coincides with the molecular response. The resulting polarization can be expressed as the multiplication of the shifted Stokes field by the molecular response function. Each part of that polarization is subsequently probed by the same part of the Stokes spectrum that was used to excite it, receiving the inverse phase shift. In the end, the amount of modulation on the pump is given by the field strength at the pump frequency and the integral of the Stokes intensity weighed by the molecular response. As only the imaginary part of the response will interfere, the total amount of modulation is just the effective absorption. It would seem that any phase shaping on the Stokes field is meaningless in this framework, e.g., if the Stokes field would be heavily chirped and the absorptions in the IR are probed consecutively in time, the total absorption is still recovered when integrated over the pulse length. From this example it can also, however, be expected that shaping would have an effect on any coherent redistribution of energy within the molecule during the pulse. Whether that signal will be large enough to be useful remains to be seen.

Selectivity and efficiency

Our shaping schemes are all aimed at generating an optimally selective response on the spectrally integrated return signal. This choice of an optimization of the integrated signal allows for simple detection that in turn allows for high-speed imaging (van Rhijn et al. 2009). Other schemes can be created (Oron et al. 2004, McGrane et al. 2009) where a larger response is generated in a limited part of the spectrum. A handwaving rule for the selectivity is that the selectivity increases with increasing complexity of the molecular response. However, the spectrum should not be so congested (homogeneously broadened) that the phase response is reduced to a slowly varying function without distinct features. Similarly, the features in the molecular response should not be narrower than the resolution of the shaper.

The efficiency of the broadband response is similar to that of narrowband CARS or SRS, where the rule is that for an efficient generation of signal the molecular response should "fill" as much of the excitation spectrum as possible. In general, this means that narrowband CARS centered on the largest peak will generate the maximum signal for a given input energy but with very little selectivity. For a given spectral width the efficiency increases with the "filling factor", which increases for more complex spectra, so that both efficiency and selectivity both go up for increasingly complex spectra, making this a potentially interesting technique for high-speed imaging with chemical selectivity.

Most broadband CARS approaches (multiplex and single pulse) and broadband SRS approaches are not aimed at high-speed imaging. They require spectrally dispersed detection which is relatively slow. Their aim is not to coherently combine the response from different vibrational resonances but rather to collect very selective information (with the exception of Oron et al. 2004). Imaging speeds are in the order of many minutes (Gilch et al. 2010, Kano 2010). This is currently still slightly lower than what can be done with fast scanning OPO systems (Sung et al. 2011). Compared to other shaping approaches our approach therefore has the potential to provide faster imaging, more like those for narrowband scanning. Currently, however, we are still at the stage where we use slow samples scanning so that we cannot substantiate any claims in this direction and our image acquisition takes many minutes rather than seconds. Another limit is the switching speed of the shaper. Our current shaper cannot fully switch to a shape in less than 200 ms so that imaging of multiple substances has to be done by taking complete images per phase shape rather than vary the phase shape per pixel or line. This can cause drift and stitching problems between the various images. The technology of pulse shaping is not a fully matured technology yet.

In general, if speed is not an issue, spontaneous Raman is much simpler and difficult to beat in terms of the total information obtained and the simplicity of the measurement.

The shaping presented here, however, can also potentially be used to pick up on vibrational redistribution that cannot be extracted from spontaneous Raman signals.

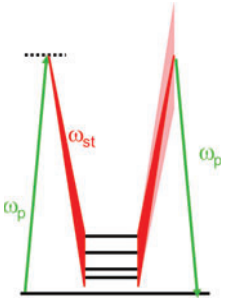

Figure 5 Energy diagram for broadband SRS with shaped pulses. The broadband Stokes profile excites a broad range in the difference frequency. An even broader polarization response is generated on the pump. However, the part that overlaps with the narrow pump is generated by probing by the same frequency as used for the excitation.

Acknowledgements

Funding for this research was provided by NanoNed, a nanotechnology program of the Dutch Ministry of Economic Affairs, by the Stichting voor Fundamenteel Onderzoek der Materie (FOM), which is financially supported by the Nederlandse Organisatie voor

Wetenschappelijk Onderzoek, NWO directly and by the Dutch Technology Foundation STW, which is the Applied Science Division of NWO, and the Technology Program of the Ministry of Economic Affairs.

References

Day, J. P. R.; Domke, K. F.; Rago, G.; Kano, H.; Hamaguchi, H.-O.; Vartiainen, E. M.; Bonn, M. Quantitative coherent anti-Stokes Raman scattering (CARS) microscopy. *J. Phys. Chem. B* **2011**, *115*, 7713–7725.

Ganikhanov, F.; Evans, C. L.; Saar, B. G.; Xie, X. S. High-sensitivity vibrational imaging with frequency modulation coherent anti-Stokes Raman scattering (FM CARS) microscopy. *Opt. Lett.* **2006**, *31*, 1872–1874.

Garbacik, E. T.; Korterik, J. P.; Otto, C.; Mukamel, S.; Herek, J. L.; Offerhaus, H. L. Background-free nonlinear microspectroscopy with vibrational molecular interferometry. *Phys. Rev. Lett.* **2011**, in press.

Gilch, P.; Ploetz, E.; Marx, B. Disturbing interference patterns in femtosecond stimulated Raman microscopy. *J. Raman Spectrosc.* **2010**, *41*, 609–613.

Jurna, M.; Korterik, J. P.; Otto, C.; Herek, J. L.; Offerhaus, H. L. Vibrational phase contrast microscopy by use of coherent anti-Stokes Raman scattering. *Phys. Rev. Lett.* **2009**, *103*, doi: 10.1103/Physrevlett.103.043905.

Jurna, M.; Garbacik, E. T.; Korterik, J. P.; Herek, J. L.; Otto, C.; Offerhaus, H. L. Visualizing resonances in the complex plane with vibrational phase contrast coherent anti-Stokes Raman scattering. *Anal. Chem.* **2010**, *82*, 7656–7659.

Kano, H. Molecular spectroscopic imaging using a white-light laser source. *B Chem. Soc. Jpn.* **2010**, *83*, 735–743.

Lee, Y. J.; Moon, D.; Migler, K. B.; Cicerone, M. T. Quantitative image analysis of broadband CARS hyperspectral images of polymer blends. *Anal. Chem.* **2011**, *83*, 2733–2739.

Lucassen, G. W. *Polarization sensitive coherent Raman spectroscopy on (bio)molecules in solutions*. PhD thesis, University of Twente, 1992.

McGrane, S. D.; Scharff, R. J.; Greenfield, M.; Moore, D. S. Coherent control of multiple vibrational excitations for optimal detection. *New J. Phys.* **2009**, *11*, doi: 10.1088/1367-2630/11/10/105047.

Motzkus, M.; Muller, C.; Buckup, T.; von Vacano, B. Heterodyne single-beam CARS microscopy. *J. Raman Spectrosc.* **2009**, *40*, 809–816.

North, D. O. An analysis of the factors which determine signal/noise discrimination in pulsed carrier systems. RCA Labs: Princeton, NJ, 1943.

Oron, D.; Dudovich, N.; Silberberg, Y. All-optical processing in coherent nonlinear spectroscopy. *Phys. Rev. A* **2004**, *70*, doi: 10.1103/Physreva.70.023415.

Orsel, K.; Garbacik, E. T.; Jurna, M.; Korterik, J. P.; Otto, C.; Herek, J. L.; Offerhaus, H. L. Heterodyne interferometric polarization coherent anti-Stokes Raman scattering (HIP-CARS) spectroscopy. *J. Raman Spectrosc.* **2010**, *41*, 1678–1681.

Parekh, S. H.; Lee, Y. J.; Aamer, K. A.; Cicerone, M. T. Label-free cellular imaging by broadband coherent anti-stokes Raman scattering microscopy. *Biophys. J.* **2010**, *99*, 2695–2704.

Potma, E. O.; Evans, C. L.; Xie, X. S. Heterodyne coherent anti-Stokes Raman scattering (CARS) imaging. *Opt. Lett.* **2006**, *31*, 241–243.

Rinia, H. A.; Bonn, M.; Muller, M.; Vartiainen, E. M. Quantitative CARS spectroscopy using the maximum entropy method: the main lipid phase transition. *Chemphyschem*. **2007**, *8*, 279–287.

Saar, B. G.; Freudiger, C. W.; Reichman, J.; Stanley, C. M.; Holtom, G. R.; Xie, X. S. Video-rate molecular imaging in vivo with stimulated Raman scattering. *Science* **2010**, *330*, 1368–1370.

Sung, J. H.; Chen, B. C.; Lim, S. H. Fast three-dimensional chemical imaging by interferometric multiplex coherent anti-Stokes Raman scattering microscopy. *J. Raman Spectrosc.* **2011**, *42*, 130–136.

Turin, G. L. An introduction to matched filters. *IRE Trans. Inform. Theory* **1960**, *6*, 18.

Umapathy, S.; Lakshmanna, A.; Mallick, B. Ultrafast Raman loss spectroscopy. *J. Raman Spectrosc.* **2009**, *40*, 235–237.

van Rhijn, A. C. W.; Postma, S.; Korterik, J. P.; Herek, J. L.; Offerhaus, H. L. Chemically selective imaging by spectral phase shaping for broadband CARS around 3000 cm^{-1}. *J. Opt. Soc. Am. B* **2009**, *26*, 559–563.

van Rhijn, A. C. W.; Jurna, M.; Jafarpour, A.; Herek, J. L.; Offerhaus, H. L. Phase-shaping strategies for coherent anti-Stokes Raman scattering. *J. Raman Spectrosc.* **2011**, *42*, doi: 10.1002/jrs.2922.

Volkmer, A.; Nandakumar, P.; Kovalev, A. Vibrational imaging based on stimulated Raman scattering microscopy. *New J. Phys.* **2009**, *11*, doi: 10.1088/1367-2630/11/3/033026.

Xie, X.S.; Freudiger, C. W.; Min,W. ; Holtom, G. R.; Xu, B.; Dantus, M. Highly specific label-free molecular imaging with spectrally tailored excitation-stimulated Raman scattering (STE-SRS) microscopy. *Nat. Photonics* **2011**, *5*, 103–109.

Xie, X. S.; Roeffaers, M. B.; Zhang, X.; Freudiger, C. W.; Saar, B. G.; van Ruijven, M.; van Dalen, G.; Xiao, C. Label-free imaging of biomolecules in food products using stimulated Raman microscopy. *J. Biomed. Opt.* **2011**, *16*, doi: 10.1117/1.3516591.

Yang, D.; Sprünken, D. P.; van Rhijn, A. C. W.; Savolainen, J.; Chen, T. L.; Offerhaus, H. L.; Herek, J. L.; Jafarpour, A. Investigation of adaptive laser pulse shaping by direct estimation of group delay profile. *Opt. Commun.* **2011**, *284*, 3748–3758.

Zheltikov, A. M.; Volkmer, A.; Radi, P. P.; Zumbusch, A. New trends and recent advances in coherent Raman microscopy and nonlinear optical spectroscopy: introduction to the special issue. *J. Raman Spectrosc.* **2009**, *40*, 712–713.

Received September 6, 2011; accepted November 30, 2011;
previously published online February 23, 2012